JOURNAL OF SPACECRAFT AND ROCKETS
Vol. 33, No. 1, January–February 1996

Spike-Nosed Projectiles with Vortex Rings: Steady and Nonsteady Flow Simulations

Ameer G. Mikhail*
U.S. Army Research Laboratory, Aberdeen Proving Ground, Maryland 21005-5066

Numerical computations are reported for a spike-nosed projectile configuration with a tripping ring. A vortex-dominated flowfield is computed at supersonic speeds of $M_\infty = 3.5$, 3.0, and 1.9. A time-dependent Navier–Stokes computational technique with zonal gridding was used. The axial force at zero angle of attack was computed and found to be in good agreement with the wind tunnel data at Mach 3.0. The wind tunnel sting effect on the axial force coefficient and the flow pattern was found to be very minor for the present case at Mach 3.5. An additional interesting case was computed at Mach 1.9, and the flow was found to be of the oscillatory (buzzing) type. The frequency of the oscillation was computed as 5333 Hz.

Nomenclature

A_{ref} = reference area, $(\pi d^2/4)$
C_D = drag coefficient, drag force/$(0.5\rho V^2 A_{\text{ref}})$
C_p = specific heat under constant pressure
C_v = specific heat under constant volume
d = reference diameter
d_s = spike diameter
e = specific total energy, $C_v T + \frac{1}{2}(u^2 + v^2)$
J = Jacobian of the coordinate transformation
M = Mach number
p = static pressure
Re = Reynolds number per foot, $\rho V_\infty/\mu$
T = temperature
u, v = velocity components in the x and y directions
V_∞ = freestream velocity
x, y = Cartesian coordinates for two-dimensional case, axial and radial coordinates for axisymmetric case
α = angle of attack
β = index equaling 1 or 0 for axisymmetric or two-dimensional case, respectively
γ = ratio of specific heats
ϵ = turbulent eddy viscosity coefficient
μ = laminar (molecular) viscosity coefficient
ξ, η = transformed coordinates in the computational plane for the coordinates x and y
ρ = density

Subscripts

0 = total (stagnation) condition
∞ = freestream condition

Introduction

SPIKE-NOSED projectile configurations are used against armored targets, where the spike provides a standoff distance between the armor and the shaped-charge warhead. These projectiles have been continuously developed and improved, despite their high-drag disadvantage. One major difficulty with the spike-nosed configurations is the possibility of two flow patterns. In many cases, one does not know which flow pattern will occur under what conditions. One flow pattern is of low drag and the other is of a higher drag. Unfortunately, the high-drag pattern is more dominant and more stable, whereas the lower drag pattern is less dominant and occurs in fewer cases. Some projectiles launched at high-supersonic speeds start with the high drag and then switch to the lower drag mode, which is more stable at a lower speed. In other cases the flow may oscillate slowly between the two modes. In other configurations the flow oscillates rapidly causing the buzzing phenomenon. The critical Mach number for switching patterns depends on the Mach number, the length of the spike, the spike diameter to projectile diameter ratio, and, to a lesser degree, the Reynolds number and flow turbulence.

Platou[1] reported the two flow patterns experienced during supersonic wind tunnel testing in the early 1950s. Koenig et al.[2] more recently reported hysteresis mode changes during transonic wind tunnel testing. Shang et al.[3] successfully and accurately simulated the buzzing phenomenon in the 1970s for a re-entry body with a relatively short spike. Calarese and Hankey[4] tested and analyzed the oscillations of spike-tipped bodies. Mikhail[5] in 1989 successfully computed the flow past three sharp-edged, spike-nosed configurations and induced the two modes for each case. Mikhail verified his results at Mach = 1.72 with the wind tunnel tests of Ref. 1.

To avoid the uncertainty of the dual flow modes, it had been found long ago that by inserting a ring near the spike tip the high drag mode is prevented. This is accomplished by introducing flow separation along the spike and preventing reattachment before the flow reaches the projectile shoulder, which causes a shoulder bow shock and the high drag. No specific name in the literature is credited for suggesting such a tripping device. This ring device should more appropriately be named vortex generator ring due to its major effect on creating a vortex-dominated flowfield, rather than to its effect on creating mere flow separation. The usual notion of tripping, induced from the laminar to turbulent boundary-layer tripping devices, is wrong. However, its use, unfortunately, is widespread among researchers.

The present study concerns itself with projectiles with tripping rings of interest to the U.S. Army. In particular, the interest is drawn from the 105-mm M490A1 spike-nosed, spin-stabilized projectile. This round is an improved training round for the 105-mm M456A1 fin-stabilized, high explosive antitank (HEAT) projectile. Computations at three different Mach numbers are performed, and the sting support effect is studied to assess its influence. The results are compared with wind tunnel data for verification. A new and interesting flow pattern was observed and is described. Also, for a high-drag case, the high-drag solution was induced by prescribing a pseudo-crossflow boundary condition as described earlier in Ref. 5. Further, a buzzing flow case was encountered, and the frequency of buzzing was computed.

Projectile Geometry and the Test Cases

The projectile configuration of interest to the U.S. Army is the 105-mm M490A1 spin-stabilized projectile version of the M490 fin-stabilized training round. Wind tunnel test results were available from Ref. 6 at only two Mach numbers, 3.0 and 3.5. The wind tunnel

Received June 19, 1994; revision received June 19, 1995; accepted for publication Aug. 8, 1995.

*Aerospace Engineer, Weapons Technology Directorate, Propulsion and Flight Division. Associate Fellow AIAA.

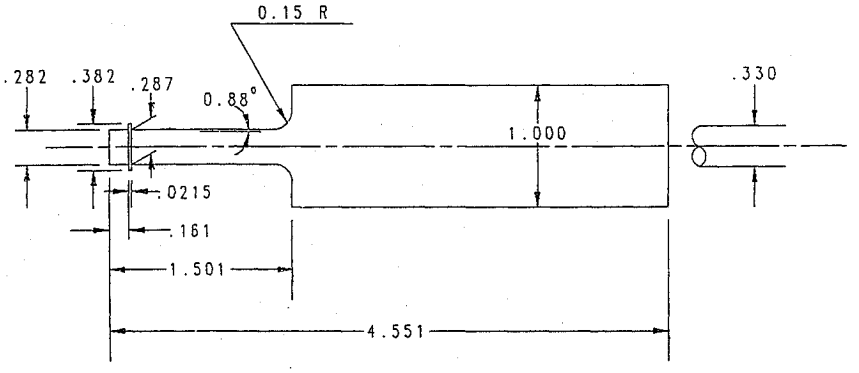

Fig. 1 Projectile wind tunnel model configuration (105-mm modified M490 training HEAT projectile, later designated M490A1). Dimensions are in calibers; 1 caliber = 2.002 in. (50.85 mm).

models were of 2.0-in. diameter, representing 48% of the full-scale projectile. Several variations in the projectile spike diameter, projectile shoulder geometry, and the afterbody were tested. The chosen configuration for the present study was model number 1112, depicted in Fig. 1. The tests were run in a blow-down supersonic wind tunnel with the following test conditions: Mach numbers 3.0 and 3.5, total pressure 60.0 and 70.0 psi, total temperature 59.0°F, and Reynolds number 10.2 and 9.1 $\times$ 10^6/ft, respectively. Some range firing tests were also made for the spinning full-scale projectile.[7] Because of the yawing motion observed and lack of documentation, the zero yaw axial force coefficient, however, was not readily available. Also note that the scaling laws between the full-scale and the 0.48-scaled models for spike-nosed bodies are not well established. The flow pattern and the flow over the spike are highly sensitive to the spike length (in association with the local Reynolds number influencing the separation region along the spike) and to the projectile shoulder diameter (the shoulder diameter to the spike diameter ratio). Therefore, the wind tunnel results were favored over the range tests for the numerical simulation.

The sting support was 0.67 in. in diameter, corresponding to 0.333 of the model base diameter. Cases of angles of attack between ± 8 deg were tested and measured. No error bounds on any of the given measurements were given in the report of Ref. 6.

Computational Technique

Governing Equations

The compressible, turbulent Navier–Stokes equations for axisymmetric and two-dimensional flow can be expressed[8] in the following strong conservation form where the dependent variables ρ, u, v, and e are mass averaged. In these equations u and v are the axial and radial velocity components, ρ and p mean density and pressure, respectively, and t time:

$$\frac{\partial Q'}{\partial t} + \frac{\partial E'}{\partial x} + \frac{\partial F'}{\partial y} + \left(\frac{F'}{y} + \frac{H'}{y}\right)\beta = 0$$

where

$$Q' = \begin{bmatrix} \rho \\ \rho u \\ \rho v \\ \rho e \end{bmatrix} \qquad E' = \begin{bmatrix} \rho u \\ \rho uu + p - \tau_{xx} \\ \rho uv - \tau_{xy} \\ (\rho e + p)u - \tau_{xx}u - \tau_{xy}v + \dot{q}_x \end{bmatrix}$$

$$F' = \begin{bmatrix} \rho v \\ \rho uv - \tau_{xy} \\ \rho vv + p - \tau_{yy} \\ (\rho e + p)v - \tau_{xy}u - \tau_{yy}v + \dot{q}_y \end{bmatrix} \qquad H' = \begin{bmatrix} 0 \\ 0 \\ -p + \sigma_+ \\ 0 \end{bmatrix}$$

$$\tau_{xx} = -\frac{2}{3}(\mu + \epsilon)\tilde{\nabla} \cdot \tilde{V} + 2(\mu + \epsilon)\frac{\partial u}{\partial x}$$

$$\tau_{xy} = (\mu + \epsilon)\left(\frac{\partial u}{\partial y} + \frac{\partial v}{\partial x}\right) \tag{1}$$

$$\tau_{yy} = -\frac{2}{3}(\mu + \epsilon)\tilde{\nabla} \cdot \tilde{V} + 2(\mu + \epsilon)\frac{\partial v}{\partial y}$$

$$\tau_{\Theta\Theta} = \sigma_+ = -\tfrac{2}{3}(\mu + \epsilon)\tilde{\nabla} \cdot \tilde{V} + 2(\mu + \epsilon)(v/y)$$

$$\tilde{\nabla} \cdot \tilde{V} = \frac{\partial u}{\partial x} + \frac{\partial v}{\partial y} + \left(\frac{v}{y}\right)\beta$$

$$\dot{q}_x = -C_p\left(\frac{\mu}{Pr} + \frac{\epsilon}{Pr_t}\right)\frac{\partial T}{\partial x}$$

$$\dot{q}_y = -C_p\left(\frac{\mu}{Pr} + \frac{\epsilon}{Pr_t}\right)\frac{\partial T}{\partial y}$$

The air is assumed to be perfect gas, satisfying the equation of state. Sutherland's law for viscosity variation with temperature is applied.

The laminar and turbulent Prandtl numbers, Pr and Pr_t, were assumed constant with values of 0.72 and 0.9, respectively. The ratio of the specific heats γ was also assumed constant and equal to 1.4.

The total energy per unit mass e is given by

$$e = C_vT + \tfrac{1}{2}(u^2 + v^2)$$

In the ξ–η computational plane, Eq. (1) is transformed to the conservation law form, and the equations can be found, for example, in Ref. 8.

Turbulence Model

Turbulence is modeled through a modification to the eddy viscosity model of Baldwin and Lomax.[9] This widely applied model employs the two-layer concept (inner and outer layers). Because of the perpendicular intersection of the spike surfaces at the nose tip and also at the facing shoulder, the normal distance to these walls y is difficult to assign.[10] This problem was approached in Ref. 10 by measuring the y along a 45-deg ray emanating from the point of intersection of the two perpendicular walls.

Computer Code

The computer code was developed by Patel and Sturek[8] and utilizes the robust explicit, time-dependent method of McCormack. The code is vectorized and is run on Cray X-MP/48 machine. The present computations, however, were all run in serial arithmetic mode. The zonal grid and overlapping is provided in the code as represented by eight different zones (can be increased if so desired). The user prescribes the overlapping between regions along one line of adjacent zones (interface). A global uniform time step was used herein rather than grid-varying time steps to simulate time-accurate solutions. The time step is determined from the Courant–Friedrichs–Lewy (CFL) condition, with a factor of 0.6 being used as the Courant number. Characteristic time lengths for the flowfield at $M = 3.0$ and 3.5 were 454 $\times$ 10^{-6} and 389 $\times$ 10^{-6} s, respectively. With an average time step of 0.19 $\times$ 10^{-6} s, the characteristic time lengths correspond to 2390 and 2050 numerical time steps at Mach = 3.0 and 3.5, respectively.

Boundary Conditions

No-slip conditions are specified on all wall surfaces. The incoming flow conditions are assumed to be of uniform profiles with freestream values based on the wind tunnel test values: M_∞ = 1.9, 3.0, and 3.5; T_∞ = 302, 185, and 150°R; P_∞ = 7.31, 1.63, and 0.98 psi; and Re = 12.62 × 10^6, 10.20 × 10^6, and 9.10 × 10^6/ft.

The outgoing flow conditions at the downstream end of the flowfield were imposed as zero gradients along the body axis direction at a distance of 4.0 body diameters behind the projectile base.

The outer boundary conditions were imposed as nonreflective conditions, i.e., zero gradient conditions along characteristic lines for all variables. The characteristic direction is determined from the local velocity and temperature. This approach allows setting the outer field close to the body without the penalty of any unnecessary approximation regarding shock reflection, or degradation due to far-field conditions (zero-gradients) being set too close.

At the symmetry line, ahead of the spike tip and behind the base, a two-point zero gradient boundary condition is imposed on the solved variables.

Initial Conditions

Computations for the first case of Mach 3.0 were started using freestream values everywhere in the computational domain for all variables, based on an initial lower Mach number that was selected as 1.5. These values are for freestream pressure and temperature. The density and specific total energy are computed accordingly, using the equation of state and the definition of the specific total energy. The rest of the cases were started in the same manner except for the case of Mach 3.5 with no sting, which was started using the converged solution for the same case with the sting at the same Mach number.

Grid

Six different grid zones were used in the computation. Those zones and the extent of the computational domain are depicted in Fig. 2.

For the case with a sting, the grids used for the six zones are (20, 85), (13, 72), (7, 65), (60, 78), (130, 36), and (80, 31). The first and second arguments in the brackets refer to the axial and radial directions, respectively. This grid is equivalent to 16,531 total points or about a 129 × 129 grid. For the case of no sting, the same grid is used except for the last zone, which was increased from 80 × 31 to 80 × 51 to account for the space previously occupied by the sting.

One restriction in the present grid overlapping technique is that no interpolation is allowed at the interface line between zones. Thus, each point on either side of any two zones must have the exact same coordinates. This restriction represents some constraint in the flexibility of the grid distribution and may be alleviated in future development of the code. Meanwhile, to accommodate this restriction one has to accept unnecessary clustering of points in some locations. Figures 3 and 4 show the overall grid distribution for the projectile configuration with and without sting, respectively. Figure 5 shows the details of the grid near the spike, depicting the clustered points along lines parallel to the top body surface where clustering is needed near the body to resolve the turbulent boundary layer.

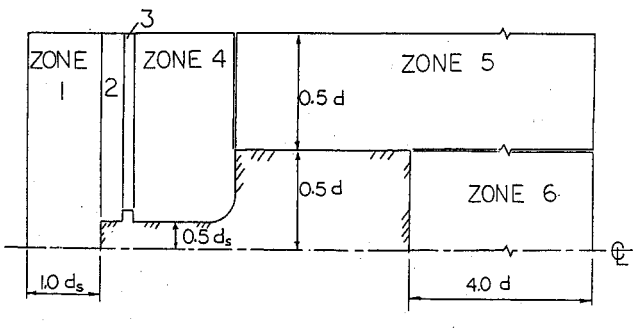

Fig. 2 Grid zones and computational domain.

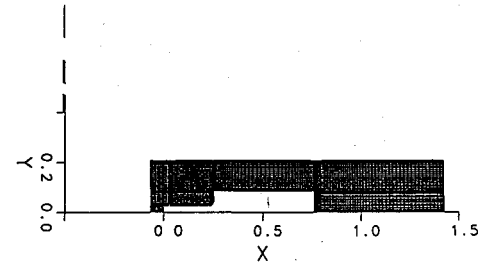

Fig. 3 Computational grid case, with a sting support.

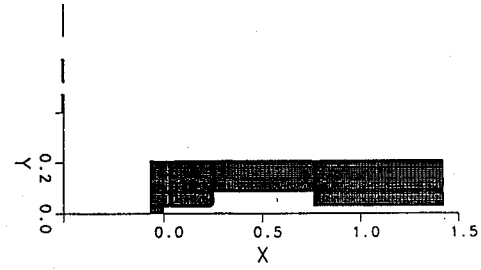

Fig. 4 Computational grid case, with no sting.

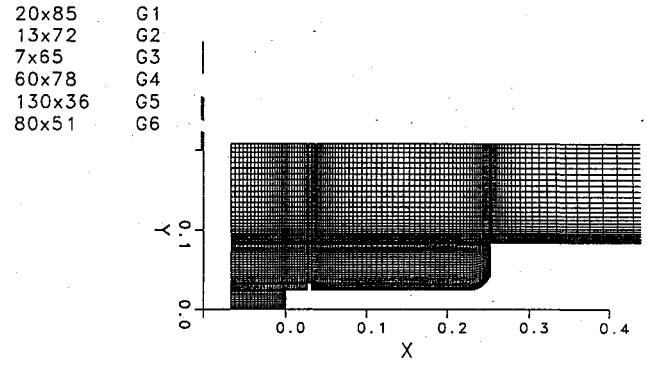

Fig. 5 Details of the grid near the spike.

Results

Case at M = 3.0

This case was started using the earlier stated initial conditions and the described grid with the sting. A new flowfield, dominated by the vortex generated by the tripping ring, extended over the projectile middle body and beyond the base of the projectile. This vortex-wake stream interfered with the usual expansion wave expected at the base for the supersonic flow. The wake flow eliminated the expansion wave and the outer supersonic flow slipped over the wake stream almost unturned; thus, no expansion wave took place. At first, this behavior was suspected but was later confirmed when the spark shadowgraph photographs for the corresponding full-scale projectile (obtained during the range test firing of Ref. 7) were reviewed. Examination of the shadowgraphs confirmed the computations and showed little trace of the expected expansion wave. In addition, the shadowgraph showed the vortex-wake region emanating from the vortex ring and flowing all of the way over the projectile body. This flowfield, now appearing to be logical and acceptable was, nevertheless, not expected. This is the first time in the known literature that such particular flowfield has been analyzed and computed. Figure 6 depicts the spark shadowgraph for the full-size 105-mm modified M490 projectile at M = 2.16 and yaw angle of 4.5 deg. There are no free flight tests that can be achieved at zero yaw angle. Therefore, the 4.5-deg yaw effect must be subtracted from the effect on the windward and leeward sides of the projectile shown. Two other similar shadowgraphs exhibited the same flow at M = 2.24 and α = 3.7 deg and at M = 1.89 with α = 3.9 deg. A schematic of the flow pattern is shown in Fig. 7 and is compared with the typical expected flow for a spiked body without a tripping ring. This vortex-dominated field effect on the expansion wave at the base was never shown in the literature and was not exposed in Mikhail's earlier

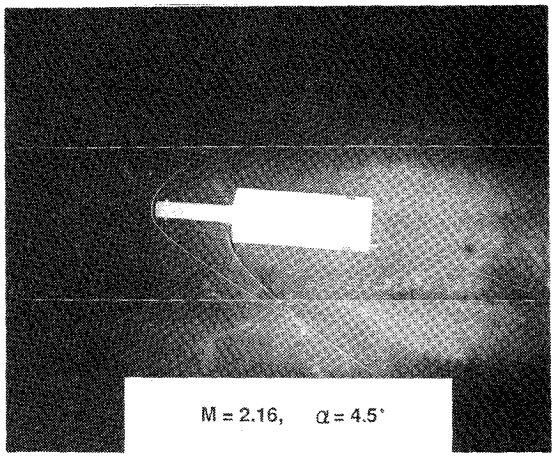

Fig. 6 Spark shadowgraph for the full size 105-mm M490A1 projectile.

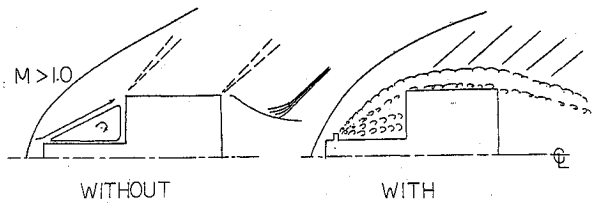

Fig. 7 Flow patterns for spiked projectiles with and without a tripping ring.

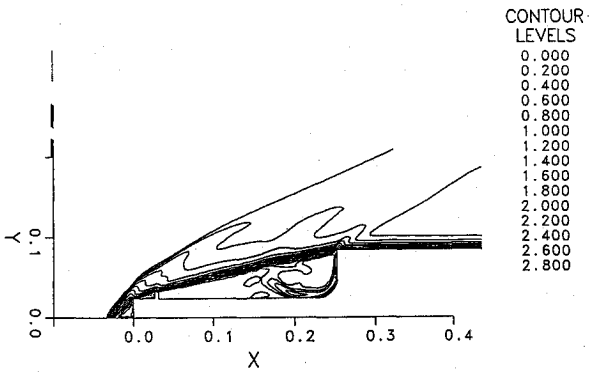

Fig. 8 Flowfield for $M = 3.0$ case, Mach-line contours near the spike tip.

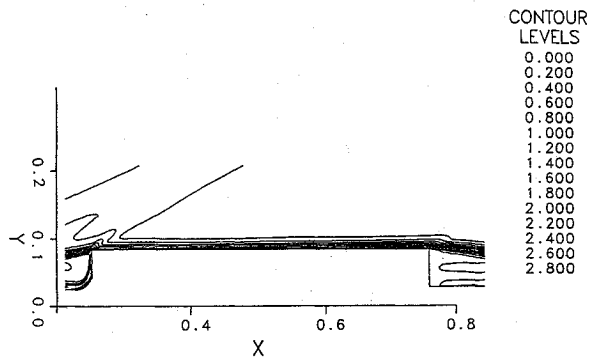

Fig. 9 Flowfield for $M = 3.0$ case, Mach-line contours near projectile shoulder.

work[5] since no base region computations were made for the spiked configurations with a tripping ring.

The flowfield is depicted in Figs. 8–10 by the Mach-line contours for the regions near the spike tip, the shoulder, and the base of the projectile. The average axial force coefficient, which here also is the drag coefficient, was computed to be 0.253, which compares extremely well with the value of 0.255 from the wind tunnel data.[6]

The case took about 40,000 time steps to converge only because there is a very small eddy continuously breaking down and reforming near the base that propagates upwind to the frontal spike tip. It is not known at this point whether this unsteadiness is truely physical or purely numerical in nature. This caused the drag coefficient to vary slightly at a slow frequency. The drag coefficient variation is provided in Fig. 11 as a drag history plot.

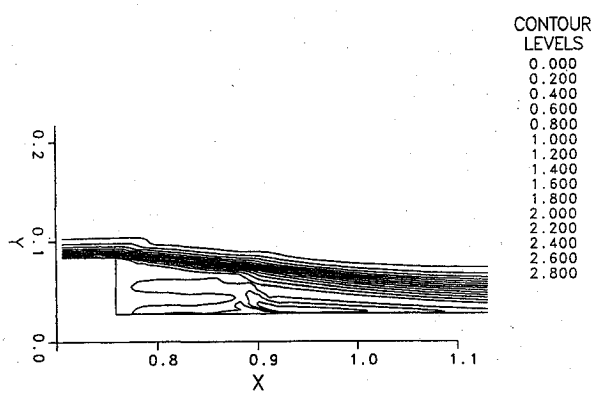

Fig. 10 Flowfield for $M = 3.0$ case, Mach-line contours near the sting support.

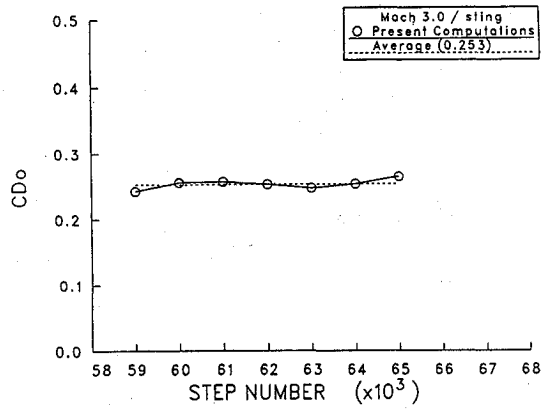

Fig. 11 Numerical conversion history for $M = 3.0$ case.

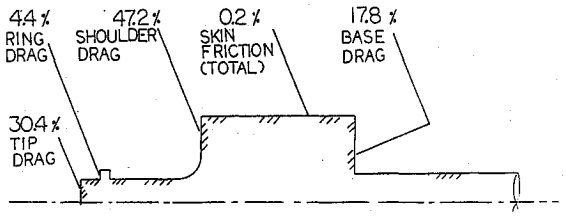

Fig. 12 Drag anatomy for $M = 3.0$ case.

Figure 12 provides the anatomy of the drag for the case at $M = 3.0$, showing the value of each component of the drag. The shoulder drag was 47%, whereas the base pressure drag was 18% of the total drag. The spike frontal area caused 30% of the total drag, whereas the skin friction of the whole body contributed a mere 0.2%. The vortex ring contributed only 4.4%.

The computation time on the Cray X-MP/48 was about 40 min for each 1000 time steps. For 40,000 steps this amounts to about 27 h of CPU time.

Case at $M = 3.5$

The case with the sting was started from the same uniform initial conditions described earlier. The case took about 58,000 steps to converge with this high number of steps due, as explained earlier, to the small eddy breakup. The computations could have been stopped at half the number of steps with no appreciable difference. It was kept running, however, first, to observe any changes and, second, to ensure that no numerical instability would occur.

The axial force coefficient computed was 0.233; as expected, that is lower than the value for the $M = 3.0$ case, since the drag decreases as supersonic Mach number increases. The tunnel test, however, provided a higher value of $C_D = 0.309$. It was immediately realized

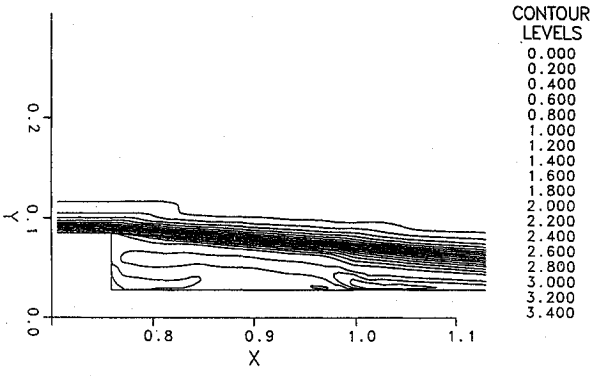

Fig. 13 Flowfield for $M = 3.5$ case, Mach-line contours for case with sting.

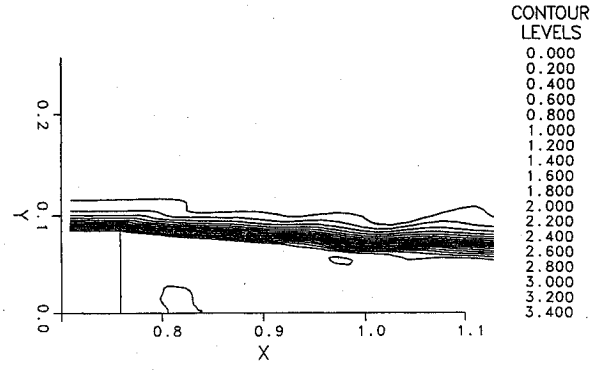

Fig. 14 Flowfield for $M = 3.5$ case, Mach-line contours for case without sting.

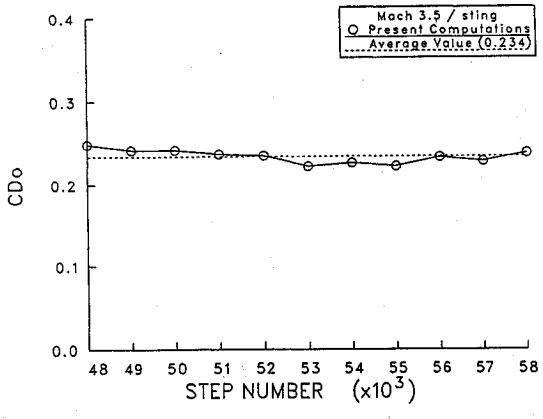

Fig. 15 Numerical convergence history for $M = 3.5$ case.

that the tunnel test resulted in the high-drag value, whereas the computation resulted in the low-drag flow pattern value. Also, the sting was suspected to influence the frontal spike flow pattern through this oscillating small structure eddy. Therefore, the effect of the sting had to be assessed first.

Effect of the Sting

The sting was removed, and the new grid replacing the space previously occupied by the sting was constructed. The new grid is depicted in Fig. 4. The solution was started from the converged values where the case with a sting ended. The computations did not take more than 10,000 steps to settle again and converge. Surprisingly, no appreciable difference was observed in the frontal spike flow or in the flow pattern. Only some changes in the base flow were observed, as expected. Two eddies near the base-sting corner disappeared when the sting was removed. The new C_D value obtained was 0.232 compared to the 0.233 for the case with the sting. The small eddy breakup also existed. The flowfield for the cases with and without sting is given in Figs. 13 and 14. The numerical convergence history for C_D is given in Fig. 15.

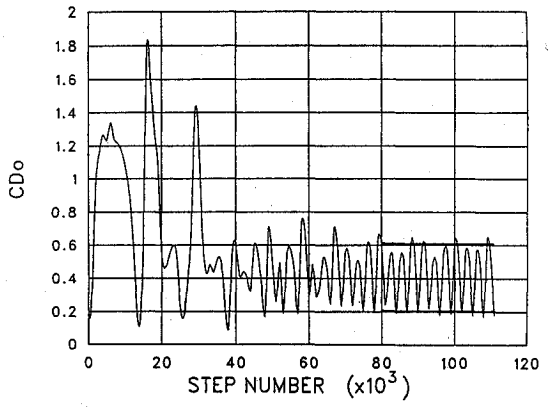

Fig. 16 Oscillatory drag coefficient for the $M = 1.9$ case.

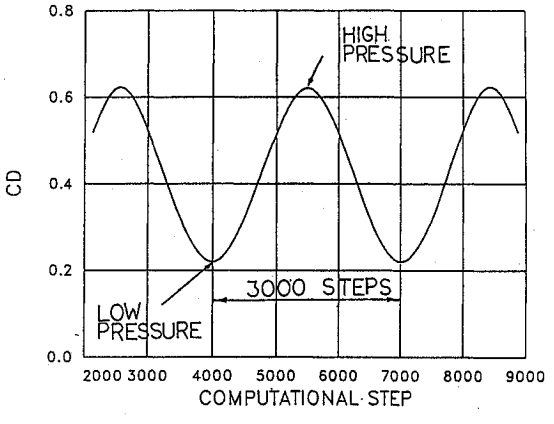

Fig. 17 Idealized oscillatory cycle for the $M = 1.9$ case.

High-Drag Case

With the computed axial force coefficient being lower than the wind tunnel value, it was necessary to compute the corresponding high-drag case. Based on the previous experience cited in Ref. 5, the high-drag mode was then induced by the method cited that suggested a pseudosimulation of the effect of an angle of attack. The computation took 30,000 steps to converge (20 h CPU time). The computed C_D was 0.347. This obtained value falls between the two wind tunnel data points of 0.309 and 0.386. The numerical convergence history is given in Fig. 17. Other possible mechanisms can also be the triggering factor for this high drag pattern, such as slight model asymmetries, numerical dissipation or turbulence modeling parameters.

Case at $M = 1.9$

After the computations of the preceding two cases, the variation of C_D with the Mach number was of interest due to the low- and high-drag cases encountered at $M = 3.5$. Although no wind tunnel data are available at lower speeds, an additional case at $M = 1.9$ was chosen for computation to assess the C_D variation with Mach number for this particular projectile configuration. Having no wind tunnel data to compare with, and after the previous result that the sting had no effect on the spike flow, the $M = 1.9$ case with no sting was computed to simulate the in-flight behavior of the projectile.

The computation started from the same uniform initial conditions and, after a large number of time steps (80,000), the solution showed a very clear type of oscillatory (buzzing) behavior. This buzzing unsteadiness is of a different class than the small unsteadiness observed earlier due to the small eddy breakup. The clear oscillatory behavior was observed to be almost cyclic after about 80,000 steps and persisted to 110,000 steps with a very constant frequency of about 3000 steps per cycle. Therefore, 10 complete cycles were encountered before the computations were stopped. This buzzing flow pattern had no constant amplitude in the pressure oscillation, attributable to the noncyclic eddy breakup. This same phenomenon is frequently observed in combustor flow applications, with and without combustion processes. For example, Jou and Menon,[11] in their study of

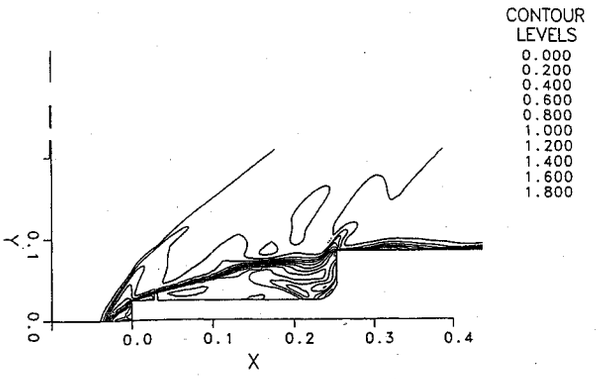

Fig. 18 Mach-line contours for the $M = 1.9$ case, near the spike tip, at high-pressure point.

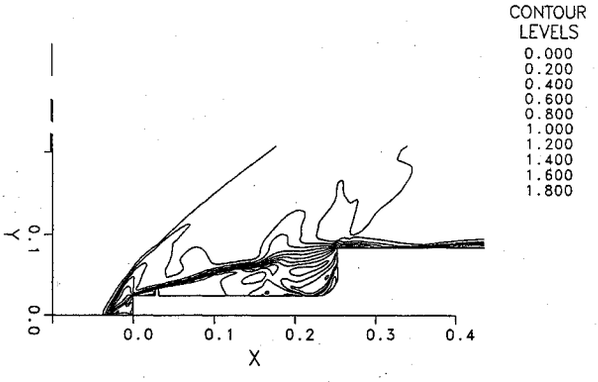

Fig. 19 Mach-line contours for the $M = 1.9$ case, near the spike tip, at low-pressure point.

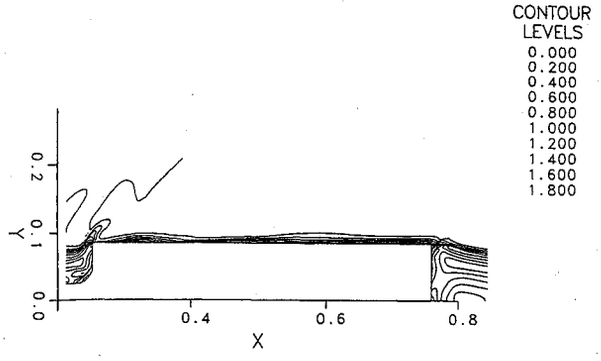

Fig. 20 Mach-line contours for the $M = 1.9$ case, near the shoulder, at high-pressure point.

nonreacting flow inside a ramjet combustor, obtained a buzzing flow with a variable pressure amplitude due to the large eddies existing in the flow past the sudden expansion section. The flow in their case oscillated with a favored frequency but with variable pressure amplitude. The phenomenon there was also explained as the effect of continuous formation and breakup of large eddies in the flow.

For the present case, with the time step $\Delta t = 0.19 \times 10^{-6}$ s, the frequency of the buzz was 5333 Hz. The drag coefficient oscillated between about 0.22 and 0.62 with a mean value of about 0.42. The flow pulsated between high-pressure and low-pressure points. The oscillatory drag behavior is depicted in Fig. 16 and the more detailed idealized oscillatory cycle is shown in Fig. 17. The variation in amplitude of the oscillation was disturbing at first, but when consulting the literature, the same behavior was readily confirmed. Jou and Menon[11] obtained a large eddy breakup pattern when computing nonreacting flow in a dump combustor. The flow in their case also oscillated with nonconstant amplitude.

The flowfield for this interesting buzzing flow is captured both at the high- and low-pressure points of the cycle. Figures 18–23 depict the flow near the spike tip, the shoulder, and the projectile base. Surprisingly, few flow differences are observed as the flow

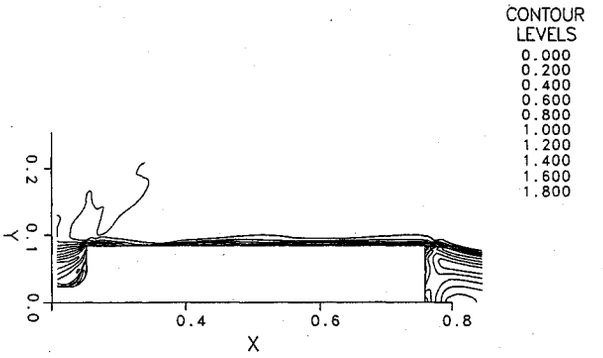

Fig. 21 Mach-line contours for the $M = 1.9$ case, near the shoulder, at low-pressure point.

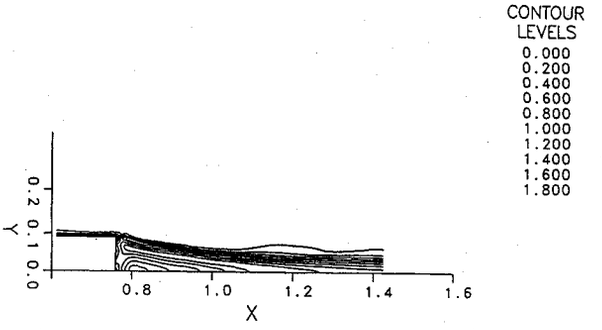

Fig. 22 Mach-line contours for the $M = 1.9$ case, near the base, at high-pressure point.

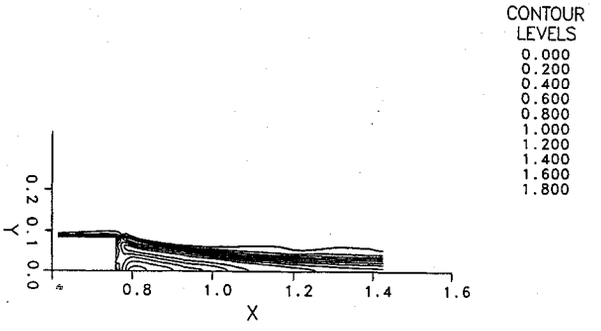

Fig. 23 Mach-line contours for the $M = 1.9$ case, near the base, at low-pressure point.

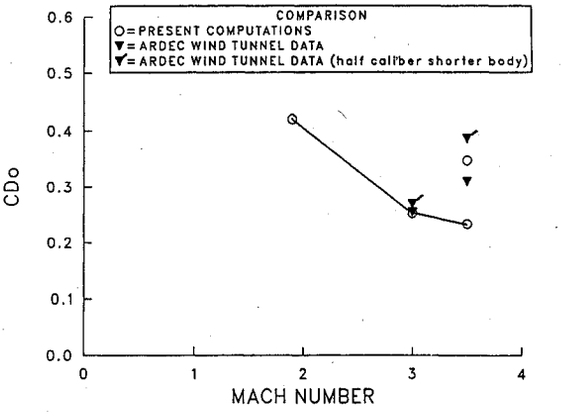

Fig. 24 Drag coefficient comparison for all cases computed.

pulsates very rapidly. The subsonic flow on the spike, impacting the body shoulder, was the main cause for the large drag changes.

Finally, the drag coefficient variation with the Mach number is depicted in Fig. 24 for all cases computed and is compared with the available wind tunnel data. The data validate the computations at Mach 3.0, whereas the computations extend the results down to Mach 1.9.

Summary and Conclusions

Five computations were made for a spike-nosed projectile with a vortex ring at Mach 1.9, 3.0, and 3.5 at zero angle of attack. The computations were made by solving Navier–Stokes equations in an overlapped zonal gridding topology, using McCormack's explicit scheme. The results obtained are summarized as follows. 1) A new flow pattern that is dominated by the vortex and wake generated by the tripping ring is computed and described. The vortex-wake field extends to the base of the projectile and interfers with the usual flow expansion there. The axial force coefficient was in excellent agreement with the wind tunnel data at Mach 3.0. 2) At Mach 3.5, both low- and high-drag patterns were obtained. 3) The sting effect on the flow pattern and axial force was studied and found to be almost nonexistent for the present sting diameter, which was only 0.33 of the projectile base diameter. The base flow pattern was slightly influenced and showed at least two eddies, which vanished when the sting was removed, for the case of Mach 3.5. 4) A detailed drag anatomy was provided, shedding an interesting light on the total drag picture of the projectile. The front spike contributed 30%, whereas the shoulder drag is 47% of the total drag for the case at Mach 3.0. 5) At the lower Mach number of 1.9, the interesting buzzing (unsteady) flow was encountered and was computed successfully. The frequency of oscillation was found to be 5333 Hz. The axial force coefficient oscillated between 0.22 and 0.62, with a mean value of 0.42. No wind tunnel tests, unfortunately, were run at that Mach number.

The numerical procedure proved to be robust and reliable once enough grid points are used. The computations proceeded in a straightforward manner and without major interruptions, adding to the previous success reported in Ref. 5 for spike-nosed bodies. Possible future improvements should consider a better turbulence model for the base region, as well as more thorough modeling for turbulence in the recirculating flow region ahead of the projectile shoulder.

Finally, it is recommended to further test the present numerical procedure on more complex spike-nosed configurations, such as for those with fin boom, boattail, and fins. Efforts are currently underway to follow up on this recommendation.

References

[1]Platou, A. S., "Body Nose Shapes for Obtaining High Static Stability," U.S. Army Ballistic Research Lab., BRL-MR-592, Aberdeen Proving Ground, MD, Feb. 1952.

[2]Koenig, K., Bridges, D. H., and Chapman, G. T., "Transonic Flow Modes of an Axisymmetric Blunt Body," AIAA Paper 88-3536, July 1988.

[3]Shang, J. S., Hankey, W. L., and Smith, R. E., "Flow Oscillations of Spike-Tipped Bodies," *AIAA Journal*, Vol. 20, No. 1, 1982, pp. 25, 26.

[4]Calarese, W., and Hankey, W. L., "Modes of Shock-Wave Oscillations on Spike-Tipped Bodies," *AIAA Journal*, Vol. 23, No. 2, 1985, pp. 185–192.

[5]Mikhail, A. G., "Spike-Nosed Projectiles: Computations and Dual Flow Modes in Supersonic Flight," U.S. Army Ballistic Research Lab., BRL-TR-3140, Aberdeen Proving Ground, MD, Aug. 1990; also *Journal of Spacecraft and Rockets*, Vol. 28, No. 4, 1991, pp. 418–424.

[6]Falkowski, E. W., and Fleming, G. C., "Aerodynamic Characteristics of the Modified 105-mm M490 Training Projectile," U.S. Army Large Caliber Weapon Systems Lab., TR ARLCD-TR-81043, Dover, NJ, April 1982.

[7]MacAllister, L. C., "Firing Range Measurements for the 105 mm Modified M490 Projectile" (unpublished), U.S. Army Ballistic Research Lab., Launch and Flight Div., Aberdeen Proving Ground, MD, July 1980.

[8]Patel, N. R., and Sturek, W. B., "Multi-Tasked Numerical Simulation of Axisymmetric Ramjet Flows Using Zonal Overlapped Grids," U.S. Army Ballistic Research Lab., BRL-MR-3834, Aberdeen Proving Ground, MD, May 1990.

[9]Baldwin, B. S., and Lomax, H., "Thin-Layer Approximation and Algebraic Model for Separated Turbulent Flows," AIAA Paper 78-257, Jan. 1978.

[10]Danberg, J. E., and Patel, N. R., "An Algebraic Turbulent Model for Flow Separation Caused by Forward and Backward Facing Steps," U.S. Army Ballistic Research Lab., BRL-MR-3791, Aberdeen Proving Ground, MD, Dec. 1989.

[11]Jou, W.-H., and Menon, S., "Large Eddy Simulation of Flow in Ramjet Combustor," *22nd JANNAF Combustion Meeting Proceeding*, Vol. 1, Chemical Propulsion Information Agency, CPIA Pub. 432, Silver Spring, MD, 1985, pp. 331–339.

T. Chrusciel
Associate Editor